

# Experimental and Computational Visualization and Frequency Measurements of the Jet Oscillation inside a Fluidic Oscillator

Uzol, O. <sup>\*1</sup> and Camci, C. <sup>\*2</sup>

<sup>\*1</sup> Graduate Research Assistant, Department of Aerospace Engineering, The Pennsylvania State University, University Park, PA 16802, USA (Currently at Department of Mechanical Engineering, The Johns Hopkins University, Baltimore MD 21218, USA)

<sup>\*2</sup> Professor, Department of Aerospace Engineering, The Pennsylvania State University, University Park, PA 16802, USA

**Abstract:** PIV measurements and computational simulations (2D, unsteady Navier-Stokes) are performed to visualize the inherently unsteady jet oscillation inside a fluidic oscillator. Both the measurements and computations are obtained for a jet exit Reynolds number of 321, based on the maximum velocity and the nozzle width at the jet exit plane. The computed jet oscillation frequency is in close agreement with the measured PIV frequency. Formation of a pressure gradient across the jet is observed from the computations. The variation of the jet oscillation frequency with jet exit Reynolds number is also determined by single sensor hot-wire measurements inside the oscillation chamber.

**Keywords:** Visualization, PIV, Jet Oscillation, Fluidic Oscillator

## 1. Introduction

Fluidic oscillators have been used as flow meters for mass flow rate measurement purposes. These are compact devices with no moving parts, simplicity of construction and low cost. The main operating principle of the fluidic oscillator is the generation of self-induced and sustained oscillations of the flow that has a frequency which is proportional to the mass flow rate. Most of the fluidic oscillator designs make use of an oscillating jet inside the device which is created by fluid mechanical interactions.

Many different design concepts are investigated and implemented for the creation of the jet oscillation. Parry et al (1991) investigated a target fluidic oscillator in which the jet oscillation is created due to the interaction of a planar jet with a bluff body, called target. The principle of operation of a similar target fluidic oscillator is explained in detail in Boucher and Mazharoglu (1988). Mansy and Williams (1989) investigated a trapped vortex pair oscillator. The jet oscillation principle for this device was mentioned to be dependent upon the formation of two counter rotating vortices that are trapped in a convergent channel. Bauer (1981) proposed another kind of fluidic oscillator which creates a jet oscillation due to the impingement of the jet on a concave wall. More recently, similar oscillators which use the same physical phenomenon have been proposed by Huang (1995) and Huang and Hocquet (1995). Fluidic oscillators have also been proposed as heat transfer augmentation devices. A pin fin cooling device called the 'oscillator fin' is investigated in detail by Uzol (2000) and Uzol and Camci (1998) as an alternative to circular pin fins. This concept is also based on Bauer's (1981) fluidic oscillator.

In this study the jet oscillation inside the fluidic oscillator proposed by Bauer (1981) is investigated in detail in order to obtain more information about the physical mechanisms that drive the jet oscillation inside the oscillation chamber. The variation of the jet oscillation frequency

with jet exit Reynolds number is determined. Both an experimental and a computational study is performed. Particle Image Velocimetry measurements and visualizations are conducted inside the oscillation chamber of the fluidic oscillator. The jet oscillation frequency is measured by hot-wire anemometry. The computational simulations are performed to obtain detailed flow physics of this device.

## 2. Fluidic Oscillator Geometry and Operation

The fluidic oscillator consists of three separate members (Figure 1). Two front members which are of elliptical cross-section are placed transversely across the passage with the major axis of the ellipse parallel to the flow direction. These two members form a tapering nozzle which is used to create a jet between them. The downstream ends of the front members are defined as downstream facing cusps which will be used for directing the oscillating jet into the flow. The third member which receives the jet from the nozzle is called the afterbody and has an upstream facing U shaped geometry. The concave wall inside the afterbody where the jet impinges and the jet oscillation occurs is called the oscillation chamber. The relative dimensions of the fluidic oscillator are also given in Figure 1.

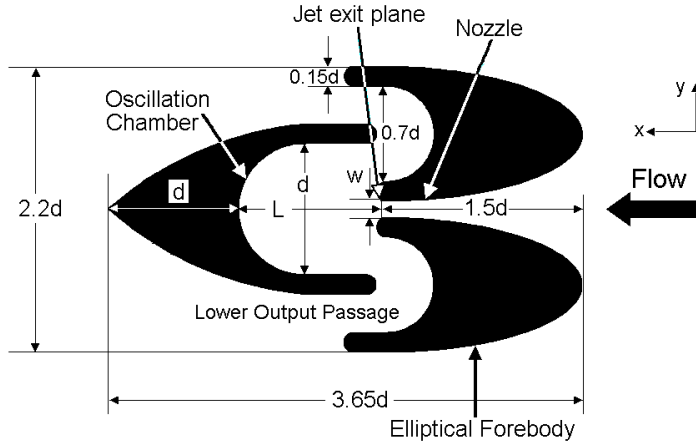


Fig. 1 The fluidic oscillator geometry used in the current jet oscillation visualization experiments and computations. The nozzle width at the jet exit plane ( $w$ ) is  $d/8$  and the distance between the jet exit plane and the oscillation chamber wall ( $L$ ) is  $9w$ .

During the operation of the fluidic oscillator, the jet coming from the nozzle impinges against the wall of the oscillation chamber and splits into two oppositely directed flows while generating two counter rotating vortices with equal magnitude of vorticity. At the very first instant the flow field inside the oscillation chamber is symmetrical. The oppositely directed flows on the upper and lower side of the jet have the same amount of mass flow rate and they exit from the upper and lower output passages, respectively. However this symmetrical layout is very unstable and any minute asymmetry in the domain results in the deflection of the jet towards one of the sides (upper or lower) and therefore destroying the symmetry. This instantly starts the inherently unsteady and periodic large scale oscillation of the jet impinging upon the concave wall. As the jet created between the two front members is swept back and forth inside the oscillation chamber, alternating flow pulses are formed and directed by cusps into the main flow.

## 3. PIV Measurements and Visualization

### 3.1 Experimental Setup

A flow visualization study inside the oscillation chamber of the fluidic oscillator is performed using particle image velocimetry to demonstrate the existence of the jet oscillation and to get some more insight to the fluidic oscillator operation. For this purpose a fluidic oscillator model with an afterbody constructed using transparent material is used in order to be able to illuminate the oscillation chamber. The experiments are conducted in the Low Speed Heat Transfer Facility at the

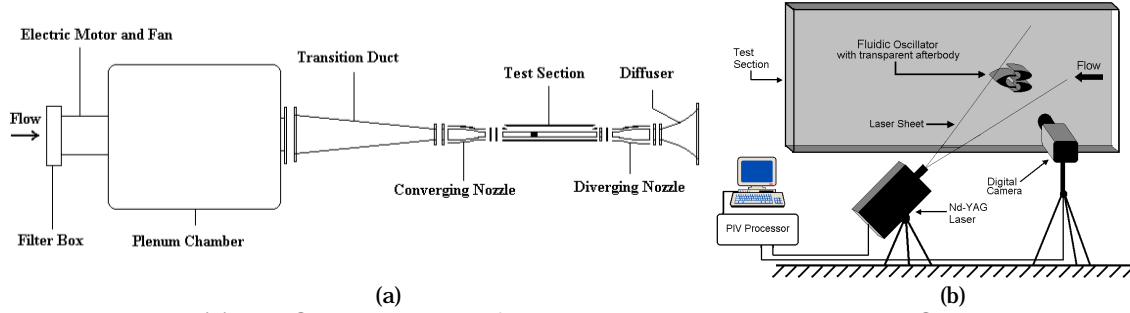


Fig 2 (a) Low Speed Heat Transfer Research Facility at Pennsylvania State University and (b) PIV measurement setup for the jet oscillation visualization inside the fluidic oscillator.

Pennsylvania State University. This is an open loop wind tunnel with an axial air blower, a diffuser with multiple screens, a plenum chamber, a high area ratio circular nozzle, a circular to rectangular transition duct, the test section and a diffuser. The test section is a 127 cm long straight rectangular duct made out of 1.27 cm thick clear acrylic and has a 36.67 cm x 7.62 cm cross-section. Figure 2a shows the experimental facility and more details about the facility can be found in Uzol (2000). The flow field is illuminated from the bottom of the tunnel test section by a double-cavity frequency-doubled pulsating Nd:YAG laser sheet which has an emitted radiation wavelength of 532 nm and 50 mJ per pulse energy level. The seeding is done using fog particles with particle sizes varying from 0.25  $\mu\text{m}$  to 60  $\mu\text{m}$ . Images of the flow field are captured using a 1k x 1k Kodak Megaplus ES 1.0 cross-correlation digital camera which is fully synchronized with the pulsating laser sheet. The PIV setup is illustrated in Figure 2b. The cross-correlation analysis of the collected PIV images are then performed using an interrogation window size of 32 x 32 pixels<sup>2</sup> with 25% overlap. The raw vector data are peak validated and then a moving average filter is applied. The experimental uncertainty error for the velocity measurements is estimated to be  $\pm 0.5\%$ .

### 3.2 Results

In order to be able to capture different phases of the jet oscillation, the experiments are conducted at a low free stream Reynolds number of 4048 calculated using the free stream velocity and the width of the fluidic oscillator. The corresponding Reynolds number at the jet exit plane inside the fluidic oscillator is 321, calculated using the maximum velocity and the nozzle width at that plane (the maximum velocity is measured using a pitot-static probe). Running at a low Reynolds number results in a low oscillation frequency which can be captured with the digital camera of the PIV system which has a maximum frequency response of 15 Hz (maximum frame rate of the camera which is utilized in the current experiments). The height of the fluidic oscillator (which is also the depth of the test section) is equal to the width of the oscillator.

Figure 3 presents instantaneous PIV particle images, the measured velocity vectors and contours of the velocity magnitude and vorticity, showing the jet oscillation inside the fluidic oscillator. The data presented is for 5 different phases of the jet oscillation and the actual time interval between each vector map in Figure 3 is 0.134s. One should keep in mind that the PIV data are recorded at 15 Hz (0.067 s time interval between vector maps). However, every other vector map is presented in Figure 3. It is observed that the jet oscillation inside the chamber is strongly periodic. While the jet is continuously fed from the nozzle, it oscillates between the lower and upper sidewalls of the oscillation chamber. One oscillation cycle is defined as the jet starting from the position that it is attached to the bottom sidewall ( $t/T=0.0$ ), continues to deflect and attaches itself to the upper sidewall and finally comes back to the position where it started ( $t/T=1.0$ ), i.e. back to the lower sidewall of the oscillation chamber. Notice that in Figure 3 at  $t/T=0.888$  ( $t=0.536\text{s}$ ), the jet has returned back to the lower sidewall, however, it is observed from the measurements that the cycle is not yet complete, i.e. the jet does not start to deflect upwards after this time step. It remains impinging upon the lower sidewall until  $t/T=1.0$  ( $t=0.603\text{s}$ , not shown). Only after this instant the oscillation cycle is completed and the jet starts to deflect towards the upper sidewall of the chamber.

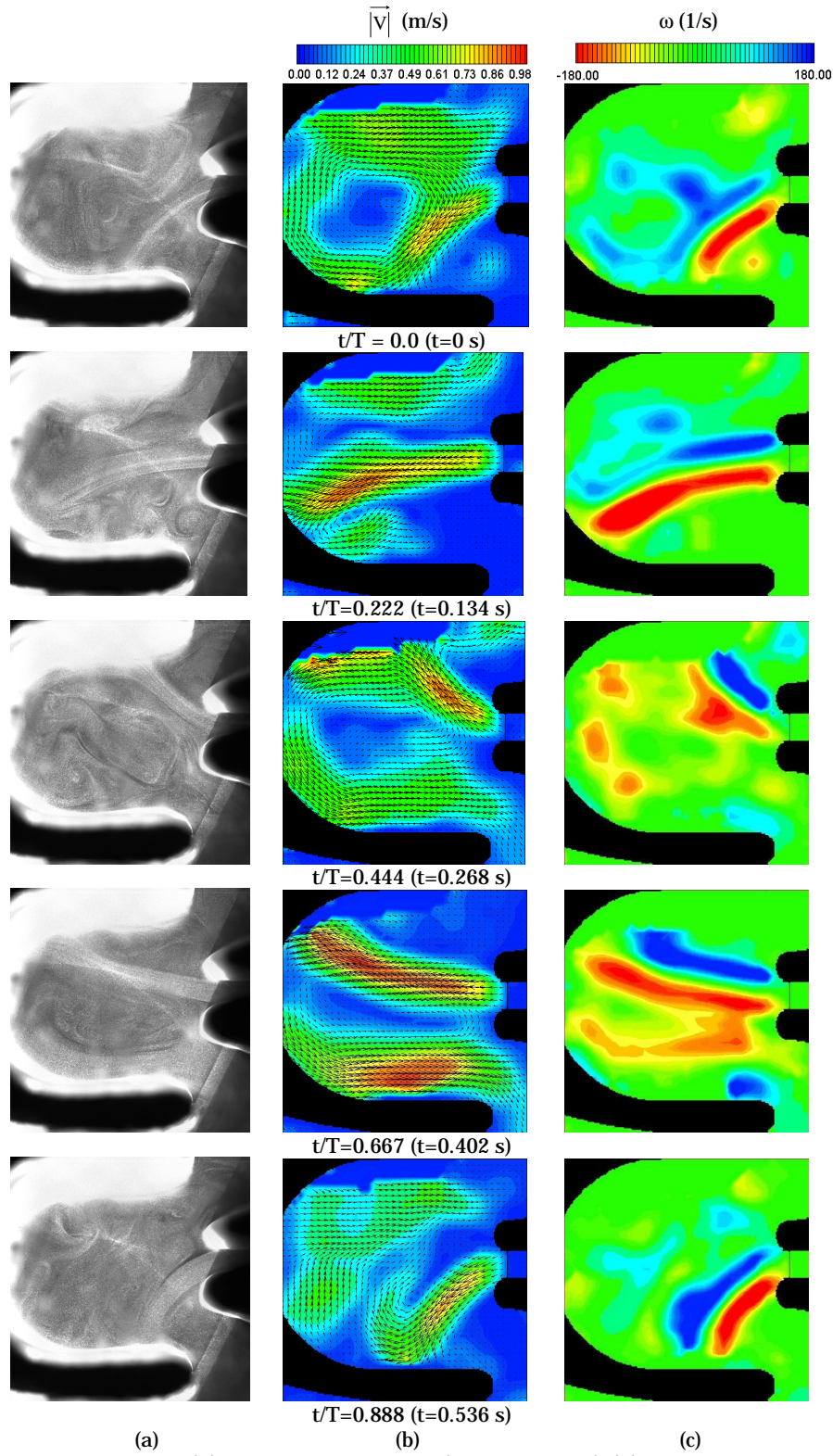


Fig. 3. Instantaneous (a) PIV particle images (one exposure) (b) Velocity vectors overlaid on velocity magnitude ( $\overrightarrow{|\mathbf{v}|}$ ) and (c) Vorticity ( $\omega$ ) contours for five different phases of the jet oscillation.  $T=0.603$  s is the period of the oscillation. Negative vorticity is out of the plane of the paper.

This corresponds to an oscillation frequency of 1.658 Hz at the current jet exit Reynolds number. These results indicate that the jet spends more time impinging on the sidewalls than transitioning between the sidewalls.

The periodic oscillation of the jet impinging on the concave wall of the oscillation chamber is visible even from the collected PIV particle images as is evident from Figure 3a. One can observe in Figure 3b and at  $t/T=0.0$  that there are two well-defined vortices on either side of the jet. At this instant the upper vortex is situated close to the center of the oscillation chamber, while the lower vortex is blocking the exit of the lower output passage. Consequently, all the incoming flow is directed towards the upper output passage and almost no flow exits from the lower output passage. The presence of these vortices is also evident in the vorticity plots. As the jet is deflected upwards from this position, the vortices become elongated and distorted and they are not as distinct as in  $t/T=0.0$ . The unsteady interaction of these two vortices at the upper and lower sides of the jet is one of the main driving mechanisms of the jet oscillation. The specific geometry of the oscillation chamber, especially the concavity of the wall and its distance from the jet exit plane are important factors in keeping the jet oscillation. Since the vortices are trapped inside the chamber and are continuously fed from the nozzle, the mutual interaction of this vortex pair drives the jet oscillation. The operation mechanism of this fluidic oscillator is actually similar to the trapped vortex pair oscillator investigated by Mansy and Williams (1989).

#### 4. Computational Simulations of the Jet Oscillation

Computational simulations of the flow field inside the oscillation chamber of the fluidic oscillator are performed in order to better understand the physics of the jet oscillation. The simulations are obtained by solving two dimensional, incompressible and unsteady Navier Stokes equations. The flow field is assumed to be laminar and constant viscosity. Hence the governing equations of the flow field are,

$$u_{i,i} = 0 \quad (1)$$

$$\rho \left( \frac{\partial u_i}{\partial t} + u_j u_{i,j} \right) = -P_i + \tau_{ij,j} \quad (2)$$

where,

$$\tau_{ij} = \mu(u_{i,j} + u_{j,i}) \quad (3)$$

Here,  $u_i$ ,  $i=1,2$  are the velocity components in  $x$  and  $y$  directions,  $\rho$  is the density,  $P$  is the static pressure,  $\mu$  is the dynamic viscosity and  $\tau_{ij}$  is the viscous stress tensor. A finite element based fluid dynamics analysis package FIDAP (1993) is used to solve the governing equations. The flow domain is discretized by nine-node quadrilateral elements which give a biquadratic velocity and bilinear pressure variation within each element. The reduced formulation for pressure, known as the 'penalty method' is used. When this method is implemented the continuity equation is discarded and the pressure is eliminated from the momentum equation using,

$$P = -\left(\frac{1}{\epsilon}\right) \nabla \cdot u \quad (4)$$

where  $\epsilon$  is the penalty parameter. Implicit backward Euler temporal formulation with a variable

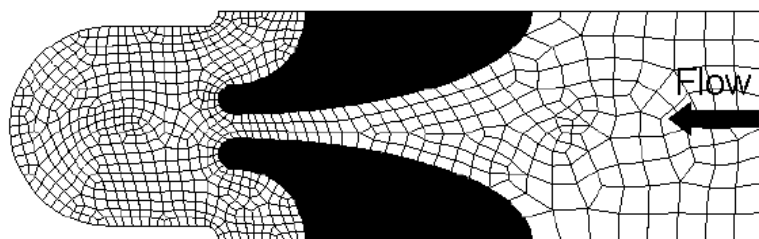


Fig. 4. Finite element mesh used for the computational simulations of the jet oscillation. 936 Nine-node second order quadrilateral elements are generated.

time increment is used for time integration. The variable time step size is controlled by a maximum local relative time truncation error of 0.1%. At each time step the equations are solved using quasi-Newton method with full reformulation on the first iteration only.

The computations are performed for a jet exit Reynolds number ( $Re_j$ ) of 321 at which the PIV flow visualization study is performed. Velocity components are specified zero on the walls in order to satisfy the no-slip condition. Since imposing an inlet boundary condition at the jet exit plane would prevent the velocity vector to change direction at that location, it would not be possible to initiate the jet oscillation inside the oscillation chamber. Instead the flow field is started upstream and the inlet boundary conditions are imposed here, so that the velocity vector at the jet exit plane could freely change direction. A uniform steady profile is imposed here such that the velocity at the jet exit plane would give the desired Reynolds number. The  $y$  component of the velocity ( $v$ ) is specified as zero at this location. No boundary conditions are explicitly imposed for velocity components at the outflow boundary. The specific form of the finite element solution procedure results in zero streamwise gradients for these variables at the outflow plane. The solution domain is discretized using 936 second order nine-node quadrilateral elements which resulted in 3247 nodes. The computational mesh is illustrated in Figure 4. The unsteady solution is started from zero velocity initial fields.

It is observed from the computational results that during the first 86 time steps (0.381 s) of the computation, the jet starts to form and slowly reach and impinge upon the concave wall of the oscillation chamber. The two vortices on either side of the jet are also slowly forming during this time period. The flow field up to this point is fully symmetrical. However after this time step the jet starts to deflect from this symmetrical position and a periodic oscillation is achieved after  $t=0.601$  s. Figure 5 presents the computed velocity magnitude, vorticity and pressure contours within the oscillation chamber during the time period in which the jet deflects from the maximum deflection point on the upper sidewall to the maximum deflection point on the lower sidewall. This time interval is actually the half period of the jet oscillation. One can notice that at  $t=0.995$  s and  $t=1.062$  s, the impingement location of the jet on the concave wall is the same. However, it is clear from the velocity magnitude and vorticity contours that there is a change in the concavity of the jet centerline, and after this instant ( $t=1.062$  s) the jet starts to deflect towards the lower sidewall. Furthermore, a sudden change in the pressure distribution around the jet is also evident from  $t=0.995$  s to  $t=1.062$  s. At  $t=0.995$  s the pressure on the lower side of the jet is lower than the pressure on the upper side. However, at  $t=1.062$  s the distribution is the opposite, i.e. lower on the upper side and higher on the lower side. This sudden change in the pressure gradient across the jet causes the change in the concavity of the jet centerline and the jet is quickly pushed towards the lower sidewall. As the jet is deflected, the pressure on the upper side continues to decrease as the vortex on this side gets bigger, while the lower vortex starts to block the output passage and causes the pressure to increase on this side. This interaction of the two counter-rotating vortices around the jet and the resulting unsteady pressure variations in the domain due to the size change and the blockage effect of these vortices are the main driving mechanisms of the oscillation. It is also observed that the maximum jet deflection angle is lower than the deflection angle observed from the PIV data.

The jet oscillation frequency as defined in the PIV flow visualization study can also be determined from the results of the computational simulations. Figure 6a shows the time history of static pressure at a point on the concave wall of the oscillation chamber and on the symmetry line. The periodic variation of the pressure is clearly visible from this figure. An FFT analysis of the pressure history (Figure 6b) gives a dominant frequency at 2.98 Hz. However during one oscillation cycle the jet sweeps this point twice. Therefore the actual jet oscillation frequency, as defined in the PIV flow visualization study, is half of this frequency which is 1.49 Hz which is underpredicted but still in close agreement with the frequency value measured in PIV experiments (1.658 Hz) for this Reynolds number. It was not possible to obtain and initiate the jet oscillation process for higher Reynolds numbers due to the need to increase the effect of the 'balancing tensor diffusivity' method of upwinding offered in FIDAP to obtain stable solutions at high Reynolds numbers. Increasing the effect of the upwinding terms for high Reynolds numbers results in an increase in false diffusion created by the upwinding scheme and hence suppresses the jet oscillation. In fact, this upwinding scheme may be the main reason behind the lower maximum deflection angles and oscillation frequency obtained from the current computations.

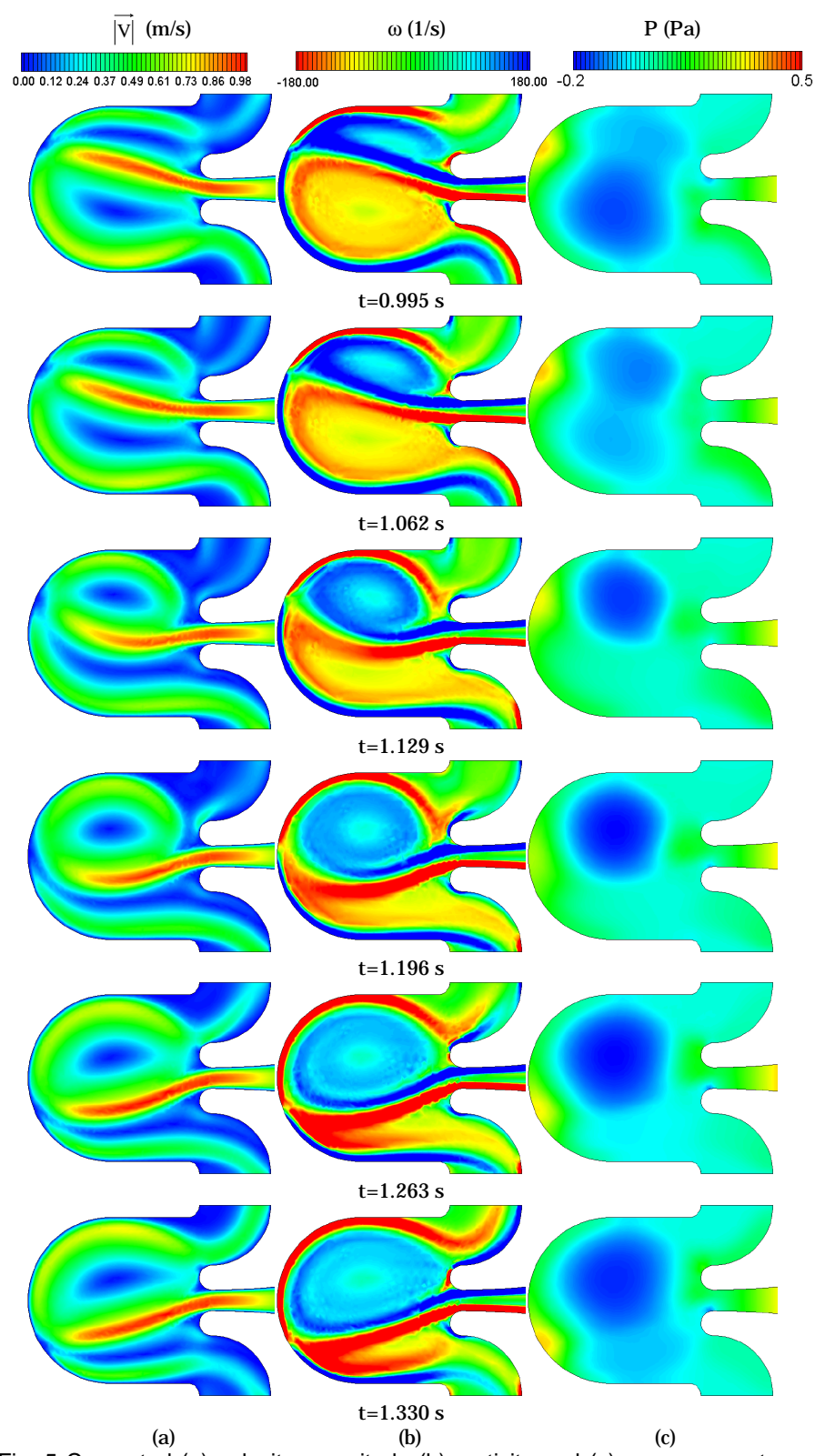


Fig. 5 Computed (a) velocity magnitude (b) vorticity and (c) pressure contours within the oscillation chamber

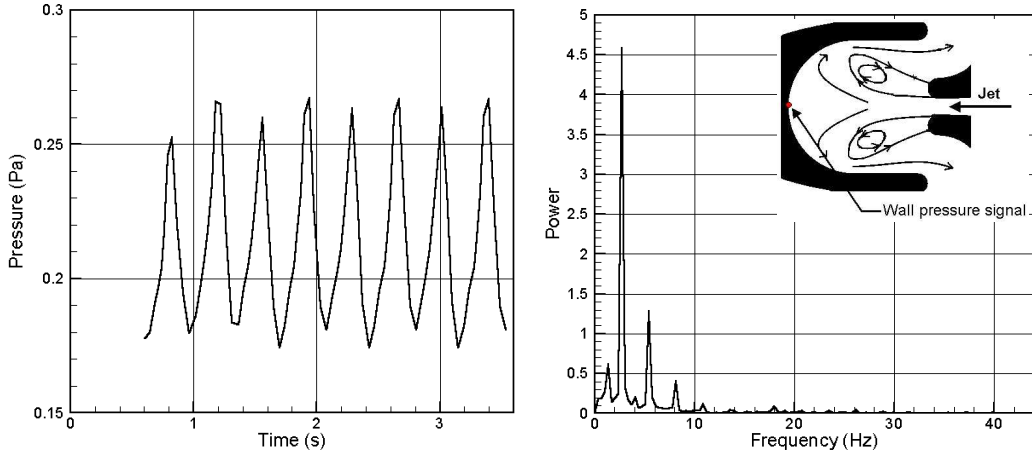


Fig. 6 (a) Time history of the pressure at a point on the concave wall and on the symmetry line of the oscillation chamber. The periodic variation due the jet oscillation starts after  $t=0.601$  s (b) FFT of the pressure signal. The dominant frequency occurs at 2.98 Hz.

## 5. Jet Oscillation Frequency Measurements

After observing the existence and the physical mechanisms of the jet oscillation inside the oscillation chamber, an experimental study is conducted to investigate the variation of the jet oscillation frequency with jet exit Reynolds number. For this purpose a single sensor hotwire probe is placed inside the oscillation chamber 15 mm (3 times the nozzle width) downstream of the jet exit plane and on the symmetry line. The location of the hot-wire probe is illustrated in Figure 7b. The single sensor hotwire probe is operated through a DISA type 55M01 single sensor hotwire anemometer system. The signal from the hotwire anemometer is first passed through a low pass filter for anti-aliasing purposes and to be able to capture the low frequency jet oscillations. The filtered signal is then fed into a digital oscilloscope and the time signature of the signal is observed for different Reynolds numbers. An online FFT analysis of the signal is also performed to capture the jet oscillation frequency which appeared as a dominant frequency in the FFT analysis.

The variation of the jet oscillation frequency and Strouhal number with the jet exit Reynolds number are given in Figures 7a and b, respectively. It is observed that the frequency varies linearly in a wide range of Reynolds numbers. The measured jet oscillation frequency for a jet exit Reynolds number of 321, at which the PIV flow visualization study is performed, is 1.6 Hz which is in agreement with the frequency observed from the PIV flow visualization study. The Strouhal number is almost constant in a wide Reynolds number range. The Strouhal number and the jet exit Reynolds number are calculated using the width of the jet exit plane and the maximum velocity measured at that plane (see Figure 7 caption).

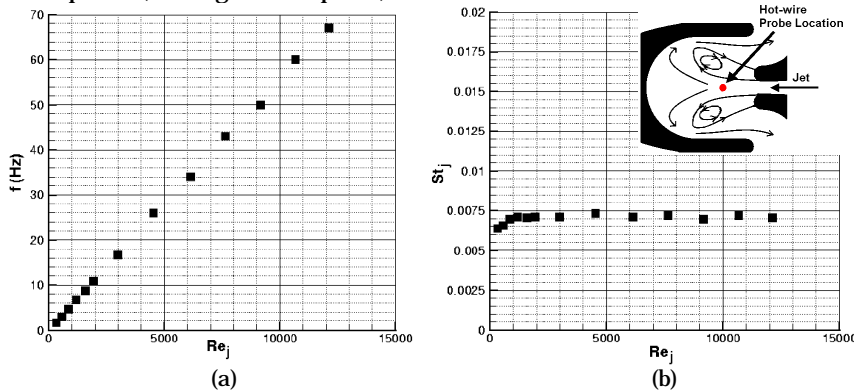


Fig. 7. Variation of the jet oscillation (a) frequency and (b) Strouhal Number with jet exit Reynolds Number ( $St_j = fw/u_j$  and  $Re_j = u_j w/v$ ,  $f$ : frequency of oscillation,  $w$ : width of the jet exit plane in Figure 1,  $u_j$ : maximum velocity at jet exit plane,  $v$ : kinematic viscosity).

## 6. Conclusions

The operation of a fluidic oscillator and the jet oscillation mechanism inside it have been studied in detail both experimentally using Particle Image Velocimetry and computationally by solving two-dimensional, unsteady Navier-Stokes equations.

The experiments reveal that the jet oscillation is strongly periodic. The unsteady interaction of the two vortices on either side of the jet is one of the main driving mechanisms of the jet oscillation. These vortices trapped within the oscillation chamber periodically change their sizes, shapes and locations as the jet is swept back and forth between the upper and lower sidewalls. The specific geometry of the oscillation chamber, especially the concavity of the wall and its distance from the jet exit plane are also important factors in keeping the jet oscillation. It is also observed that the jet spends more time impinging on the sidewalls than transitioning between the sidewalls during one period of oscillation.

The jet oscillation is also captured by solving two-dimensional, unsteady Navier-Stokes equations for the oscillation chamber. The results show an unsteady variation of the pressure field around the jet as the two vortices continuously change sizes and locations. A change in the concavity of the jet centerline is observed at the upper and lower maximum deflection points just before the jet starts to move back towards to symmetry line. This change in the concavity is mainly due to the sudden switch in the pressure gradient pattern across the jet at the maximum deflection points. Similar to the PIV data, the computational results also show that the jet spends more time at the maximum deflection points than transitioning between the points. Once the jet attaches itself to the upper or lower sidewalls, it keeps impinging on that location until the switch in the pressure gradient occurs after which the jet quickly starts to deflect towards the opposite sidewall. When the jet is at its maximum deflection point, the blockage of the output passage by one of the vortices is an important factor in this switching pattern.

The jet oscillation frequencies obtained from the PIV and hot-wire measurements and the computations are in close agreement, however the frequency is underpredicted in the computations. The reason for this may be the effect of the “balancing tensor diffusivity” method of upwinding offered in FIDAP to obtain stable solutions at high Reynolds numbers. Although the computations are performed at a low Reynolds number, there is still a certain amount of false diffusion created due to the upwinding method and this results in a lower oscillation frequency and lower jet deflection angles. The frequency measurements with hot-wire probe shows that the frequency varies linearly in a wide range of jet exit Reynolds numbers and that produces an almost constant jet Strouhal number variation in the Reynolds number range.

## References

- Bauer P., 1980, “Fluidic Oscillator and Spray Forming Output Chamber,” United States Patent No. 4,184,636.
- Bauer P., 1981, “Fluidic Oscillator Flowmeter,” United States Patent No. 4,244,230.
- Boucher R.F., Mazharoglu C., 1988, “Low Reynolds Number Fluidic Flowmetering,” *J. Phys. E. Sci. Instrum.*, Vol. 21, pp. 977-989.
- FIDAP 7.0, 1993, Users Manual, Fluid Dynamics International Inc.
- Huang B.T., 1995, “Flowmeter Having a Fluidic Oscillator,” United States Patent No. 5,396,809.
- Huang B.T., Hocquet J., 1995, “Fluidic Oscillator,” United States Patent No. 5,396,808 .
- Mansy H., Williams D.R., 1989, “An Experimental and Numerical Study of Trapped Vortex Pair Fluidic Flowmeter,” ASME FED Forum on Turbulent Flows, Vol. 76, pp. 35-39.
- Parry A. J., Chiwanga S.G., Kalsi H.S., Jepson P., 1991, “Numerical and Experimental Visualization of Flow Through a Target Fluidic Oscillator,” ASME FED Experimental and Numerical Flow Visualization, Vol.128, pp. 327-334.
- Uzol O., Camci C., 1998, “Oscillator Fin as a Novel Heat Transfer Augmentation Device for Gas Turbine Blade Cooling Applications,” Proceedings of ASME Turbo Expo 1998, Stockholm, Sweden.
- Uzol O., 2000, “Novel Concepts and Geometries as Alternatives to Conventional Circular Pin Fins for Gas Turbine Blade Cooling Applications,” Ph.D. Thesis, Pennsylvania State University, University Park, PA, USA.